Acta Biomaterialia xxx (2016) xxx–xxx

Contents lists available at ScienceDirect

Acta Biomaterialia

journal homepage: www.elsevier.com/locate/actabiomat

Full length article

Inkjet printed periodical micropatterns made of inert alumina ceramics induce contact guidance and stimulate osteogenic differentiation of mesenchymal stromal cells

Ines Lauria [a,*], Michael Kramer [b], Teresa Schröder [a], Sebastian Kant [c], Anne Hausmann [a], Frederik Böke [a], Rudolf Leube [c], Rainer Telle [b], Horst Fischer [a,*]

[a] Department of Dental Materials and Biomaterials Research, RWTH Aachen University Hospital, Pauwelsstrasse 30, 52074 Aachen, Germany
[b] Department of Ceramics and Refractory Materials, Institute of Mineral Engineering, RWTH Aachen University, Mauerstrasse 5, 52064 Aachen, Germany
[c] Department of Molecular and Cellular Anatomy, RWTH Aachen University Hospital, Wendlingweg 2, 52057 Aachen, Germany

ARTICLE INFO

Article history:
Received 12 February 2016
Received in revised form 1 July 2016
Accepted 3 August 2016
Available online xxxx

Keywords:
Alumina
Microstructures
Stem cells
Additive manufacturing
Direct inkjet printing

ABSTRACT

Bioinert high performance ceramics exhibit detrimental features for implant components with direct bone contact because of their low osseointegrating capability. We hypothesized that periodical microstructures made of inert alumina ceramics can influence the osteogenic differentiation of human mesenchymal stromal cells (hMSC). In this study, we manufactured pillared arrays made of alumina ceramics with periodicities as low as 100 μm and pillar heights of 40 μm employing direct inkjet printing (DIP) technique. The response of hMSC to the microstructured surfaces was monitored by measuring cell morphology, viability and formation of focal adhesion complexes. Osteogenic differentiation of hMSCs was investigated by alkaline phosphatase activity, mineralization assays and expression analysis of respective markers. We demonstrated that MSCs react to the pillars with contact guidance. Subsequently, cells grow onto and form connections between the microstructures, and at the same time are directly attached to the pillars as shown by focal adhesion stainings. Cells build up tissue-like constructs with heights up to the micropillars resulting in increased cell viability and osteogenic differentiating properties. We conclude that periodical micropatterns on the micrometer scale made of inert alumina ceramics can mediate focal adhesion dependent cell adhesion and stimulate osteogenic differentiation of hMSCs.

1. Introduction

High performance ceramics like alumina (Al_2O_3) exhibit high strength and wear resistance, and are especially suitable for articulating components of joint implants [1,2]. Due to its bioinert properties alumina, like other high performance ceramics, is not capable of stimulating bone formation and osseointegration both of which are major issues for implants with direct bone contact [3]. However, high performance ceramics are still respected to be convenient implant materials e.g. because of their tooth-like color in dental implantology [4]. Numerous approaches have been employed to bioactivate alumina surfaces, e. g. by inorganic coatings like hydroxyapatite or bioglass [5], hydroxylation [6], and immobilization of biomolecules [7–10]. Changing the chemical composition of the surface with other molecules such as crosslinkers to introduce biomolecules seems feasible on a small scale. However, strict regulations associated with these pharmaceutically active surfaces have prompted implant developers to explore alternative solutions yielding similar results.

Since it is known that material topography such as roughness or structured surfaces influence cellular responses, cell-material interface modifications are used extensively for metallic and ceramic materials [11,12]. Modifying techniques include anodization [13], acid etching [14], particle blasting [14,15], plasma spraying [16], and ionic [17] and electron beam radiation [18], which have been used to produce ripples, grooves, or pillars within the micrometer, submicrometer or nanometer range. Some of these techniques result only in random-like surface structures, impairing any interpretations of observed cell responses. It has also been found that surface topography is capable of enhancing the

* Corresponding authors.
E-mail addresses: ilauria@ukaachen.de (I. Lauria), Kramer@ghi.rwth-aachen.de (M. Kramer), teresa.schroeder@gmx.com (T. Schröder), skant@ukaachen.de (S. Kant), akorsten@gmx.de (A. Hausmann), fboeke@ukaachen.de (F. Böke), rleube@ukaachen.de (R. Leube), telle@ghi.rwth-aachen.de (R. Telle), hfischer@ukaachen.de (H. Fischer).

http://dx.doi.org/10.1016/j.actbio.2016.08.004
1742-7061/

response of neighboring cells in an *in vivo* situation [19,20]. Pedimonte et al. induced nanopores by anodization and observed that osteoblast cell lines showed enhanced adherence and activity [21]. Pores of alumina substrates with sizes of 20 nm and 100 nm affected mesenchymal stromal cell proliferation, morphology, expression of adhesion proteins, and osteogenic differentiation [22]. Nadeem et al. produced 50 μm grooves using embossing techniques and observed higher levels of osteonectin, bone morphogenic protein receptor 2, and osteocalcin in hMSCs, however their 10 μm groove resulted in cell alignment but no effect on osteogenesis [23]. Micropits mimicking osteoclast resorption pits revealed elevated expressions of osteopontin and increased mineralization [24]. Microgrooves fabricated by micromolding with progressively increasing ridge and groove widths enhanced the osteogenic differentiation of hMSCs validated by ALP activities, mineralization, and gene levels of osterix, ALP, osteopontin, RUNX2, and osteocalcin with 180 μm alumina grooves exhibiting the highest levels [25]. Despite moderately roughened alumina-toughened zirconia implant surfaces being well accepted by rat bone tissues, the osseointegration process seems to proceed more slowly compared to titanium [26].

To tailor ceramic surfaces further, direct ink writing [27], an additive manufacturing technique developed as a processing tool to build complex 3D structures [27–31], has been employed. Droplet-based techniques include the direct inkjet printing (DIP) process, in which two kinds of print heads for this drop-on-demand printing can be used: piezoelectric and thermal [28]. In piezoelectric head systems, a volumetric change in the fluid reservoir is induced by the application of a voltage pulse to a piezoelectric element [31]. Thermal systems have a heating element as a thin-film resistor. When an electrical pulse is applied at the head, a high current passes through the resistor and the fluid in contact with it is vaporized, resulting in increased pressure which ejects a droplet through the nozzle [32]. Three-dimensional structures require a continuous distribution of material and this necessitates contact and adhesion between individual drops after printing [29]. Droplet size can be varied by adjusting the applied temperature gradient, pulse frequency, solid content and ink viscosity [33–35]. Özkol et al. proposed that, in contrast to other printing technologies, thermal DIP allows high resolution and accuracy [30]. Drawbacks of this technique are the dimensional constraints by the small building platform, with typical sizes around 50 mm × 100 mm, limiting the production capabilities to small, detailed objects. Furthermore, accuracy limitations are a constant concern, both by agglomeration of particles within the ejection chamber as well as clogging of the nozzle. However, the dropwise buildup is able to generate very fine microstructures on numerous surfaces. Overall, the application of 3D printing in medicine could provide benefits, including cost-effectiveness and the customization and personalization of medical products [36,37].

In this study, micropillar arrays made of alumina ceramics were designed and fabricated with two different micropatterns with pillar distances of 100 or 300 μm. We hypothesized that such periodical microstructures made of inert alumina ceramics would not only be able to induce contact guidance but also could stimulate the viability and osteogenic differentiation of human mesenchymal stromal cells (hMSCs).

2. Materials and methods

2.1. Fabrication of alumina specimens

Using an alumina powder (CT 3000 LS SG, Almatis, Ludwigshafen, Germany), a slurry was synthesized to slip cast disc-shaped substrates with a green body diameter of 14.5 mm. After drying, the samples were subsequently ground using silicon nitride abrasive paper with grades 100 and 1000 respectively to a thickness of approximately 1 mm. Final grinding was performed with conventional paper sheet and inspections via stereo microscope (Stemi 2000-CS, Carl Zeiss, Jena, Germany) until no optically visible scratches could be detected. The micropatterning was performed using a prototype printing system for Direct Inkjet Printing (DIP) [36]. Alumina (CT 3000 LS SG, Almatis GmbH, Germany) was processed in a high energy mill (MicroCer, Netsch-Group, Selb, Germany) until a particle size of D50 = 0.4 μm with a narrow particle distribution was measured using laser granulometry (Mastersizer 2000 W, Malvern Instruments, Worcestershire, GK). The suspension was dispersed in aqueous medium using a dispersant based on polyacrylic and carboxylic acid. The physical properties of the suspension were adjusted by the addition of ethanol (Merck, Darmstadt, Germany) and glycerol (Glycerol 85%, Hedinger, Stuttgart, Germany). The printing was done according to the thermal drop-on-demand principle with individual print heads. Each print head provided approximately 300 nozzles of 27 μm diameter arranged in two rows, resulting in a resolution of 600 dpi. Based on these conditions, the suspension was applied directly onto the substrates using a bitmap file to build up the corresponding micropillar arrays. Due to the repetitive behavior within the cross sections of the chosen structure the same bitmap file was used for each printed layer. After processing, a short debinding step was integrated into the subsequent sintering step. The alumina samples were cleaned for reuse using ultrasonic treatment in ethanol three times for 1 min, followed by two cleanings in pure water for 1 min. The samples with printed surfaces were sterilized at 180 °C for 2 h. After osteogenic induction experiments, samples were additionally treated with 16% (v/v) HCl, heated to 80 °C and gently shaken. Subsequently, the samples were cleaned three times in pure water by ultrasonic treatment and sterilized as described above. The microstructures were then controlled by scanning electron microscopy (SEM) to ensure integrity, and the ground samples additionally controlled by contact angle measurements before and after the cleaning.

2.2. Cell culture

Human mesenchymal stromal cells (hMSC) were isolated from the femoral heads of patients receiving hip joint arthroplasty after informed consent approved by the Ethics Committee of RWTH Aachen University Hospital (EK 300/13) [38,39]. Isolation of hMSCs was carried out according to the minimum criteria of the International Society of Cellular Therapy. Single-cell suspension was prepared by flushing the spongiosa several times with hMSC growth medium (Mesenpan, PAN Biotech, Aidenbach, Germany) containing 2% FCS (Pan Biotech, Aidenbach, Germany) and 1% penicillin/streptomycin (Gibco, Invitrogen, Carlsbad, CA) using a 22 g-needle and plating the cells after centrifugation in a T75 culture flask (VWR, Radnor, USA). After 24 h, non-adherent (hematopoietic) cells were removed by medium change. Adherent spindle-shaped cells were recovered from the primary culture after 4–7 days. All cells were cultured at 37 °C, in 5% CO_2 and 90% humidity. Adherent hMSCs in culture were expanded to 5000 cells/cm^2 in hMSC growth medium. The medium was changed twice per week and cells were not used when older than passage three. Stromal cells were tested for their activity to proliferate and to differentiate into osteoblasts measured by mineral formation (see Chapter 2.3). Cell viability was measured by the ability of cells to reduce resazurin to fluorescent resorufin using the CellTiter-Blue assay (Promega, Fitchburg, USA) according to the manufacturer's instructions. An increase in fluorescence correlates with cellular growth and this assay is therefore applied to estimate cell proliferation [40].

Please cite this article in press as: I. Lauria et al., Inkjet printed periodical micropatterns made of inert alumina ceramics induce contact guidance and stimulate osteogenic differentiation of mesenchymal stromal cells, Acta Biomater. (2016), http://dx.doi.org/10.1016/j.actbio.2016.08.004

2.3. Osteogenic differentiation

One day after seeding 31,000 cells/cm^2, osteogenic differentiation was initiated by moving the cells to osteogenic induction medium (=OIM, DMEM (#D6046, Sigma-Aldrich, St. Louis, MO, USA), including 10% FCS (Pan Biotech, Aidenbach, Germany), 10 mM sodium βglycerophosphate, 100 nM dexamethasone, and 0.05 mM L-ascorbic acid 2-phosphate (Sigma-Aldrich, St. Louis, MO, USA). The medium was changed three times per week over a period of 14–21 days. At day 21, cell culture supernatants were harvested, centrifuged to remove cell debris and stored at −80 °C until the analysis of alkaline phosphatase (ALP) activity was conducted. ALP was calculated by a colorimetric assay (#ab83369, Abcam, Cambridge, UK) according to the manufacturer's instructions. Calcium mineral formation was stained using Alizarin Red S (ARS, Sigma-Aldrich, St. Louis, MO, USA), quantified and normalized to DNA concentrations in the lysates measured by picoGreen (Invitrogen, Carlsbad, USA). In brief, the cells were fixed in 100% ice-cold ethanol for 1 h at −20 °C. Then, they were rinsed with water several times and stained with 40 mM ARS/NaOH pH 4.1 for 20 min at RT. Excess staining solution was rinsed away several times with water. To solubilize calcium complexes, 800 µl of 10% (v/v) acetic acid was added and the samples were gently shaken for 30 min. Subsequently, the cell layers and supernatants were transferred to tubes, heated to 85 °C for 10 min and cooled on ice for 5 min. All samples were pelleted at 20,000×g for 15 min, and 500 µl of the supernatants were pipetted into 200 µl 10% (v/v) ammonium hydroxide. Absorbance at 405 nm was measured in duplicates from 150 µl. The cell lysate was frozen at −80 °C for DNA concentration determination using Quant-iT PicoGreen dsDNA Assay Kit (Thermo Fisher Scientific, Waltham, USA).

2.4. Real-time PCR (qPCR)

Isolation of total RNA from cell cultures was carried out using the RNeasy Mini Kit together with the QIAshredder homogenizer (Qiagen, Hilden, Germany) according to the manufacturer's instructions, and 0.5–0.8 µg RNA served as a template for the cDNA synthesis by the First Strand cDNA Synthesis Kit (#K1612, Thermo Fisher Scientific, Waltham, USA). The concentration of cDNA was evaluated using the Quant-iT PicoGreen dsDNA Assay Kit (Thermo Fisher Scientific, Waltham, USA) and the cDNA was diluted in nuclease free water (Carl Roth, Karlsruhe, Germany) to 4.5 ng/µl. Semi-quantitative real-time PCR (qPCR) was then performed with 1 µl cDNA and gene specific oligonucleotides mixed with the Universal Mastermix (Diagenode, Liège, Belgium) according to the manufacturer's instructions, on the qPCR machine Rotor-Gene Q and analyzed by Rotor-Gene Q Series Software Version 2.3.1 (Qiagen, Hilden, Germany). PCR efficiencies for each individual primer pair of target and reference genes (β-actin) were evaluated at least twice. The fold change of gene expression was calculated using the averaged efficiencies according to the Pfaffl method [41]. Primer sequences and annealing temperatures of β-actin (ACTB), ALP (ALPL/TNSALP), collagen I (COL1A1) and RUNX2 were published in [42]. Cycling was performed 40 times with 95 °C 15 s, and 60 °C for 60 s. For the analysis of osteopontin (OPN/SPP1) gene expression, the QuantiTect Primer Assay (#QT01008798, Hs-SPP1-1-SG, Qiagen, Hilden Germany) was used. The qPCR was run as mentioned above, SYBR green fluorescence was detected after an additional step at 75 °C for 5 s.

2.5. Laserscanning microscopy (LSM)

The three-dimensional profile of the periodical ceramic microstructures was characterized by LSM and software-assisted line scan analysis (Keyence VK-X 100 series). The width (x), the distance (y) and the height (z) (Supplementary (Suppl.) Fig. S1) were evaluated from five samples, and from each of the samples one random region of interest served to test nine structures, three each from left top, middle and bottom. For the five ground surface images the average roughness R_a-values were determined (n = 45).

2.6. Scanning electron microscopy (SEM)

In the next step, alumina specimens were coated with a thin gold film using a high vacuum sputter coater (SCD 020, Oerlikon Balzers Coating, Liechtenstein) and imaged on a scanning electron microscope (Leo 440i, LEO Electron Microscopy, GB). Human MSCs were seeded on 15 mm-diameter alumina samples. After 3, 7, and 21 days of incubation, cells were fixed to the samples with 3% glutaraldehyde for at least 24 h in sodium phosphate buffer (0.1 M, Merck, Darmstadt, Germany), dehydrated in an ascending ethanol series and air dried or dried with HMDS (hexamethyldisilazane, Sigma-Aldrich, Steinheim, Germany). Prior to SEM imaging using the FEI-Philips XL30 ESEM FEG, a 12.5 nm gold film was deposited on the insulating alumina surfaces using Leica EM SCD500 high vacuum sputter coater to avoid sample charging. For the analysis of mineral formation by EDX, alumina samples were not coated.

2.7. Fluorescence microscopy

Human MSCs were seeded at a density of 5000 cells/cm^2 and incubated in growth medium for five days, then washed once with prewarmed PBS and fixed with 4% (w/v) paraformaldehyde/PBS (Sigma-Aldrich, Steinheim, Germany) for 15 min. The cells were permeabilized in 0.1% Triton X-100/PBS for 3–5 min, washed twice with PBS, and incubated with 1% BSA/PBS for 30 min. Vinculin (mouse monoclonal, 1:5000 in 0.5% BSA/PBS, MAB3574, Merck Millipore, Darmstadt, Germany) and integrin-β5 (rabbit monoclonal, 1:200 in 0.5% BSA/PBS, D24A5, #3629S, Cell Signaling, Danvers, USA) were stained by incubation for 45, or 60 min, respectively, and washed three times with 0.5% BSA/PBS. Secondary anti-mouse (donkey, Alexa555, 1:2000 in 0.5% BSA/PBS, #A31570, Life Technologies, Carlsbad, USA) and anti-rabbit (donkey, Alexa555, 1:1000 in 0.5% BSA/PBS, #A31572, Life Technologies, Carlsbad, USA) were incubated for 40 min and rinsed three times with 0.5% BSA/PBS. For staining of focal adhesion kinase (FAK), the cells were fixed as described above and subsequently treated with ice-cold acetone for 30 s. Then, the cells were permeabilized as described, blocking was performed using PBS/Roti-ImmunoBlock 0.1 x (Carl Roth, Karlsruhe, Germany) for 30 min, and antibodies against FAK (mouse monoclonal, 1:400 in PBS/Roti-ImmunoBlock 0.1 x, #05-537, Merck Millipore, Darmstadt, Germany) were incubated for 1 h. Samples were rinsed three times with PBS and afterwards incubated with secondary antibodies coupled to Alexa555, anti-mouse or -rabbit (see above), diluted 1:1000 in PBS/Roti-ImmunoBlock 0.1 x and incubated for 40 min. After antibody staining, filamentous actin was visualized by binding with Phalloidin-Alexa488 for 20 min (1:50 in 1% BSA/PBS, #A12379, Life Technologies, Carlsbad, USA). Samples were finally washed three times with PBS and mounted in ProLong Gold Antifade Mountant with DAPI (#P36935, Life Technologies, Carlsbad, USA) stored in the dark until imaging at 4 °C. Stacks of fluorescence micrographs with a distance of 0.275 µm between optical slices were recorded with an Apotome.2 microscope setup (Carl Zeiss, Jena, Germany). Afterwards, contrast was enhanced for each individual optical slice using ImageJ 5.7, maximal intensity projections were calculated using Zen software (Carl Zeiss, Jena, Germany) and 3D-models were rendered using Amira 5 (FEI, Hillsboro, USA).

Please cite this article in press as: I. Lauria et al., Inkjet printed periodical micropatterns made of inert alumina ceramics induce contact guidance and stimulate osteogenic differentiation of mesenchymal stromal cells, Acta Biomater. (2016), http://dx.doi.org/10.1016/j.actbio.2016.08.004

2.8. Experimental design, analysis and statistics

Unless otherwise stated, for each individual experiment a minimum of three replicate alumina specimens were used to yield biological material. The cell culture experiments were repeated independently with hMSCs of individual donors. Values in this study are given as means of the independent experiments ± standard error of the mean. For statistical analysis using OriginPro 8.6 Software (OriginLab, Northampton, USA), a Friedman ANOVA was performed. Whenever statistical significance was evaluated a post hoc two-tailed student *t*-test was performed comparing the various alumina samples. The *p*-values <0.05 were considered statistically significant and labeled with an asterisk. All figures were prepared using CorelDRAW Graphics Suite X6 (Corel Corporation, Ottawa, Canada).

3. Results

3.1. Characterization of microstructures fabricated by direct inkjet printing

Microstructures were printed onto ground surfaces, sintered and analyzed using scanning electron microscopy (SEM) (Fig. 1A). Fig. 1B depicts the profiles of the various alumina samples investigated by laser scanning microscopy (LSM), which was used to determine that the roughness R_a value of ground surfaces was <1.8 µm. LSM was also used to investigate the dimensions of the fabricated inkjet-printed microstructures. The widths, the distances, and heights (x, y, z, respectively, see Suppl. Fig. S1) of the structures were measured by software-assisted line scan analysis of randomly chosen image sections. Pillars with distances of 111 µm, heights of 41 µm and widths of 70 µm were produced and are referred to as "100 µm structures", and pillars with 333 µm distances, heights of 32 and widths of 89 µm were produced and are referred to as "300 µm" further on in the manuscript.

3.2. Morphology of cells on microstructured alumina surfaces

Metabolic activity and LDH release of L-929 and MG-63 cell lines was not significantly affected excluding any cytotoxic effect of printed microstructures (Suppl. Fig. S2A/B). A staining of the osteoblast-like cell line MG-63 cells with Fluorescein diacetate (FDA)/propidiumiodide (PI) and hematoxylin showed that MG-63 partially oriented towards the pillar structures (Suppl. Fig. S2C). All following experiments were performed with human mesenchymal stromal cells (hMSCs) capable of differentiating into osteoblast lineages. First, hMSCs were subjected to SEM analysis of the early cellular responses (Fig. 2). On ground surfaces, after three and seven days cells spread normally and formed many pseudopodia.

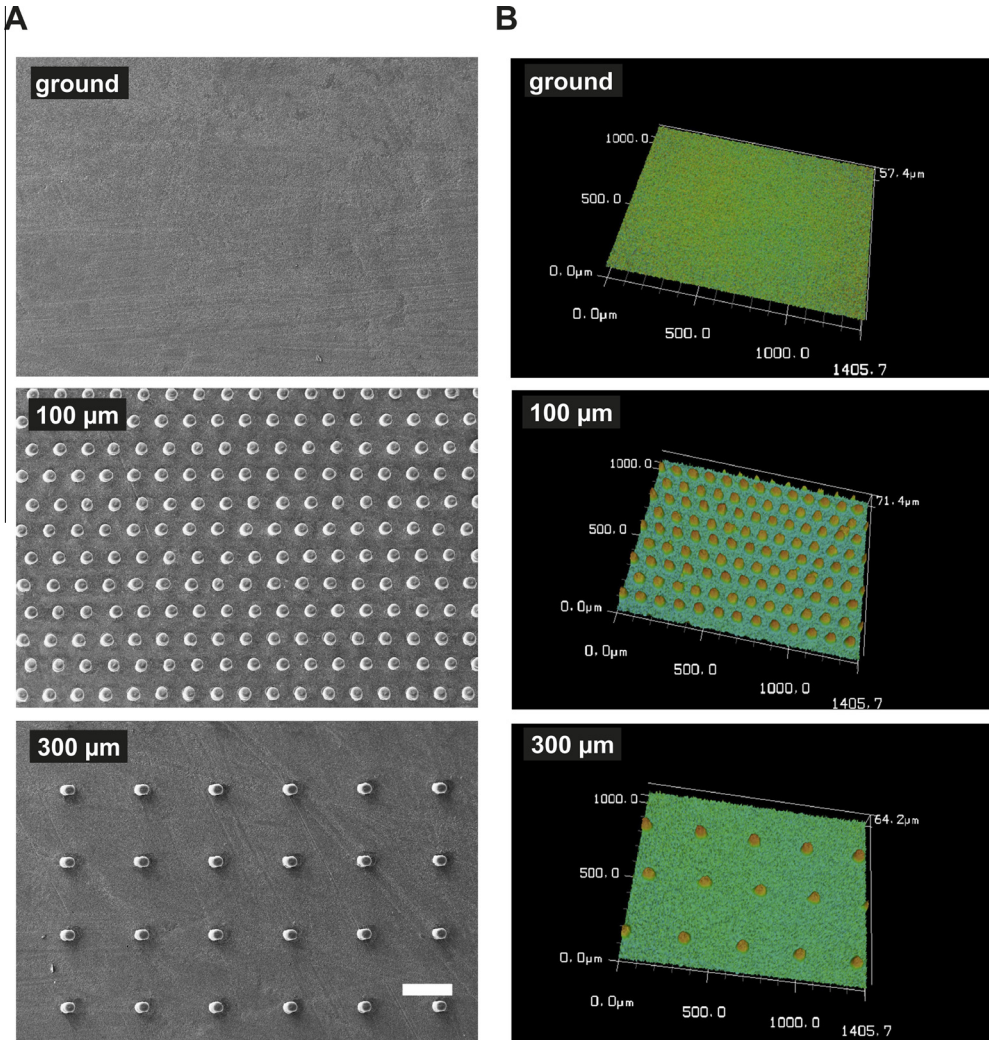

Fig. 1. Topographical analysis of pillar array structures. (A) SEM micrograph of microstructured alumina surfaces. The scale bar represents 200 µm. (B) 3D profile as determined by LSM which was used to calculate structure dimensions and the roughness R_a value of the ground surface (R_a < 1.8 µm).

Please cite this article in press as: I. Lauria et al., Inkjet printed periodical micropatterns made of inert alumina ceramics induce contact guidance and stimulate osteogenic differentiation of mesenchymal stromal cells, Acta Biomater. (2016), http://dx.doi.org/10.1016/j.actbio.2016.08.004

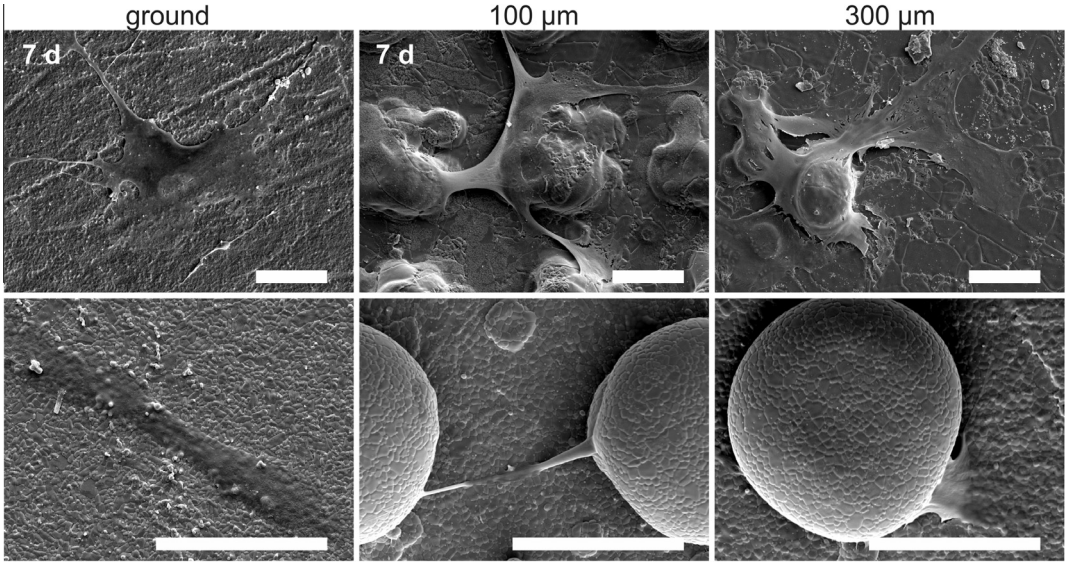

Fig. 2. Contact guidance of hMSCs. Scanning electron micrographs of hMSCs, incubated for 3 or 7 days in growth medium, fixed, dehydrated in ethanol and dried. The scale bars represent 50 µm, respectively.

Cells on printed pillar structures also spread, specifically, after three days a minor fraction of cells aligned to these structures. After seven days, the majority of the cells were able to adapt to the pillars, and on the 100 µm sample cells formed connections between neighboring structures. In the space between the surface and the printed pillars, few cells spanned the structures, indicating pillar mediated contact guidance and a directed cell migration towards and onto the structure.

After 21 days (Fig. 3 and Suppl. Fig. S3), hMSCs on ground, as well as on a polished control surface ($R_a < 0.2$ µm), formed a confluent cell layer. Notably, on the 300 µm structure, whenever cells were in close contact to a structure they grew onto it and spanned

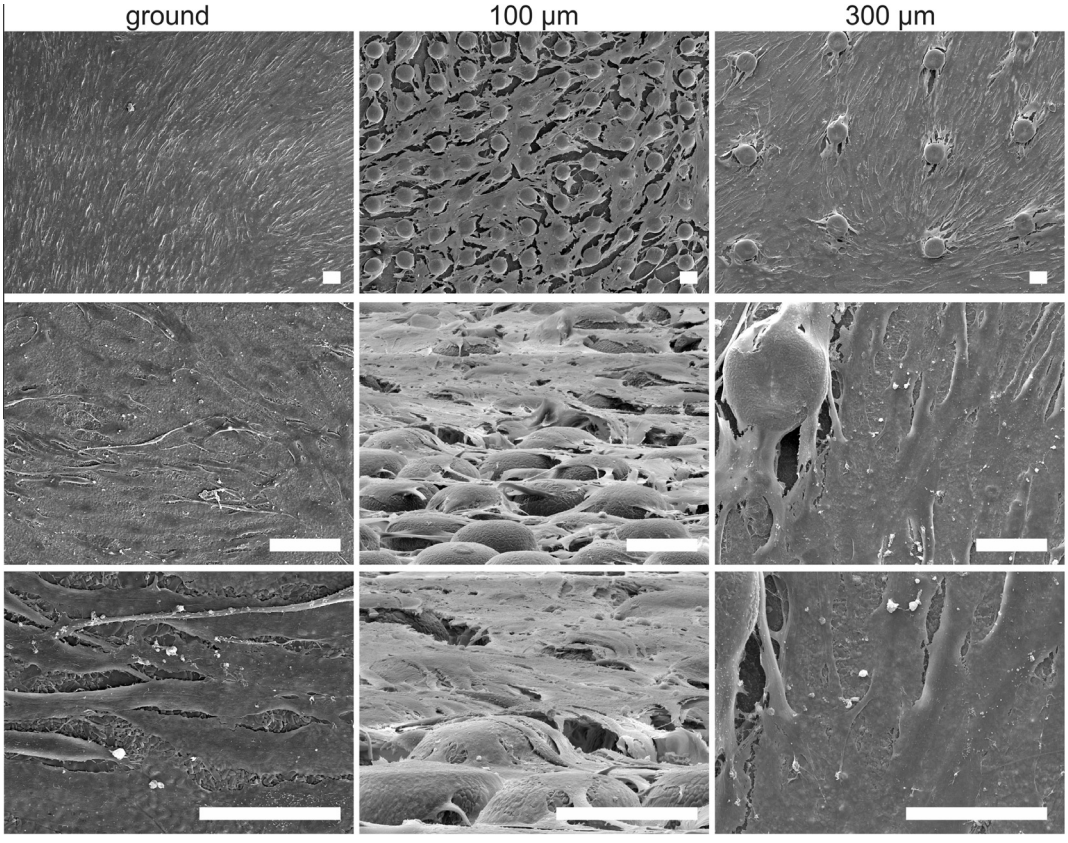

Fig. 3. Morphology of hMSC cells after 21 days. SEM micrographs of hMSCs seeded onto the various surfaces, cultured with GM. After 21 d cells were fixed, dehydrated in ethanol and dried with HMDS. The samples of the 100 µm samples were for higher magnifications hold at an oblique angle illustrating the 3D cell-material scaffold. Scale bars represent 50 µm.

Please cite this article in press as: I. Lauria et al., Inkjet printed periodical micropatterns made of inert alumina ceramics induce contact guidance and stimulate osteogenic differentiation of mesenchymal stromal cells, Acta Biomater. (2016), http://dx.doi.org/10.1016/j.actbio.2016.08.004

it as already observed earlier. Moreover, on the 100 µm printed structures hMSCs were capable of building up layers of cells between the pillars, growing considerably higher than the pillars themselves and generating a 3D scaffold built up by inorganic microstructures and organic cell mass.

To clarify whether the cell morphology as observed by SEM coincides with an attachment of cells to the micropillars, double immunofluorescence microscopy of integrin-β5, vinculin, or focal adhesion kinase (FAK) together with filamentous actin was carried out (Fig. 4, and Suppl. Fig. S4). Likewise, on polished, ground, and

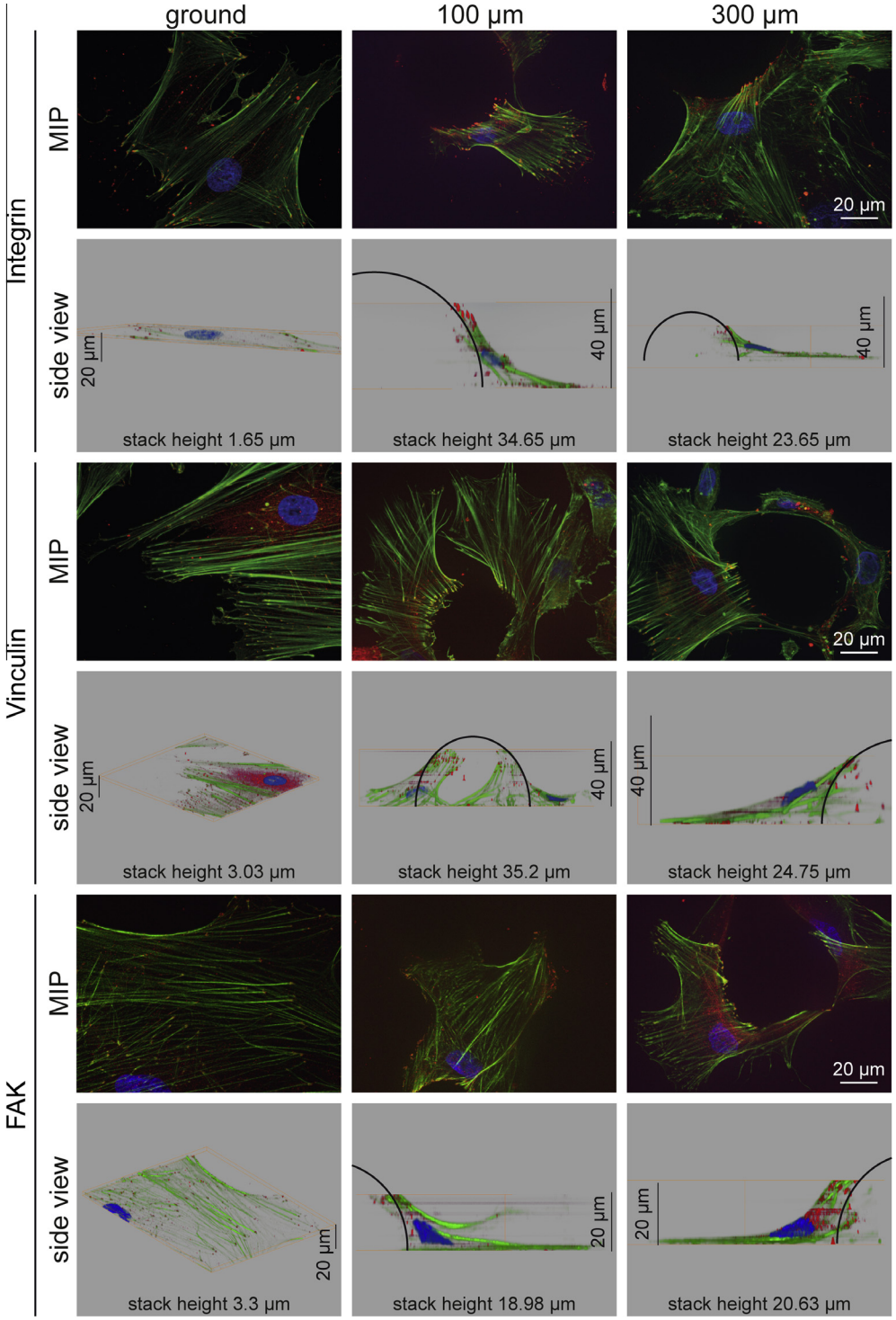

Fig. 4. MSCs form focal adhesions on the micropillars. Cells were cultured for five days, and focal adhesions were visualized by staining of integrin-β5, vinculin, or FAK (Alexa555, red) together with filamentous actin (Alexa488, green). Samples were mounted, simultaneously DAPI (blue) stained and imaged with the Apotome.2 microscope setup. Contrast was enhanced using ImageJ, and MIP was calculated by Zen software. z-Stacks were subjected to the 3D image processing software Amira. To generate side views of processed z-stacks the rendered 3D-models were flipped by 90 degree and a snapshot was taken (side view). MIP, maximum intensity projection. Black lines indicate the surface of printed microstructures.

Please cite this article in press as: I. Lauria et al., Inkjet printed periodical micropatterns made of inert alumina ceramics induce contact guidance and stimulate osteogenic differentiation of mesenchymal stromal cells, Acta Biomater. (2016), http://dx.doi.org/10.1016/j.actbio.2016.08.004

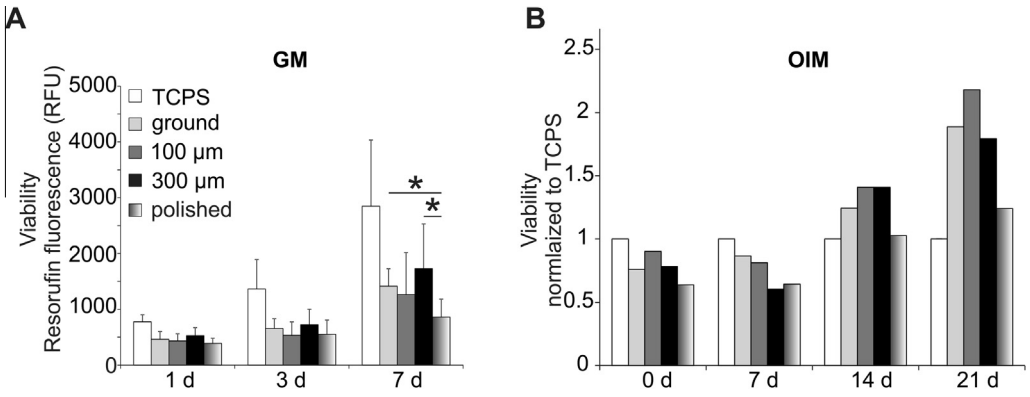

Fig. 5. Viability of hMSCs on periodically microstructured alumina surfaces. (A) Cells were seeded on alumina specimens at a density of 5000/cm^2 and treated with growth medium (GM). *, $p < 0.05$, ground ($R_a < 1.8$ µm) vs. polished ($R_a < 0.2$ µm)/300 µm vs. polished. (B) Viability monitored under osteogenic induction (OIM) conditions. The cultivation with OIM started 24 h after seeding (0 d) at a higher density of 31′000 cells/cm^2 following cultivation over 21 d. Bars represent the averaged values ± standard error derived from independent experiments with four (A) or two (B) donors using 3–6 alumina samples per day.

printed microstructured surfaces, hMSCs were widespread and filamentous actin (green) was present in all cells. On polished and ground specimens actin fibers were mostly parallel, whereas in contact with pillared microstructures actin formed thick and stretched fibers, aligning to or embracing the printed structures. The integrin staining (red) observed at the end of actin fibers demonstrated formation of adhesion complexes and thus attachment of cells to the surface. Immunofluorescent labeling of vinculin and FAK, components of focal adhesions (FAs), confirmed that these complexes were FAs. On polished and ground surfaces, FAs resided at the bottom at the cell material interface. When growing onto the micropillars, cells were directly attached to them.

3.3. Viability and proliferation of hMSCs on microstructured alumina surfaces

Assuming that cell morphology correlates with cellular activity, the cell viability was measured by metabolic activity of hMSCs at the respective time points (Fig. 5A). Excluding any effect by submicrometer structures on the ground surfaces with $R_a < 1.8$ µm, polished alumina specimens with $R_a < 0.2$ µm were also tested. Tissue culture polystyrene (TCPS) was employed as a positive control since isolation and maintenance of hMSCs was implemented on TCPS. Alumina reduced the metabolic activity of hMSCs at day 1 by up to 40%, indicating a diminished cell adhesion leading to a reduced metabolic activity of hMSCs on alumina. Day 3 did not reveal any significant difference between alumina surfaces. However, after 7 days the ground and the pillar structures with distances of 300 µm, displayed significantly higher metabolic activities compared to polished surfaces. This indicates that submicrometer structures together with 300 µm spaced microstructures stimulate cell viability of hMSCs after 7 days. Furthermore, cells seeded at higher densities and incubated with OIM for 14 days on structured surfaces exhibited elevated viability compared to TCPS and polished control, both showing similar fluorescence intensities (Fig. 5B). After 21 days, cells on 100 µm printed surfaces yielded the strongest metabolic activity.

3.4. Characterization of osteogenic differentiation

To analyze osteogenic differentiation after 21 days, ALP activity was verified in the supernatants (Fig. 6A), and matrix mineralization was confirmed and quantified by Alizarin Red S (Fig. 6B/Suppl. Fig. S5A). Present mineral crystals could be visualized by SEM and analyzed further by EDX (Suppl. Fig. S5B). ALP activities were not significantly altered under osteogenic induction conditions.

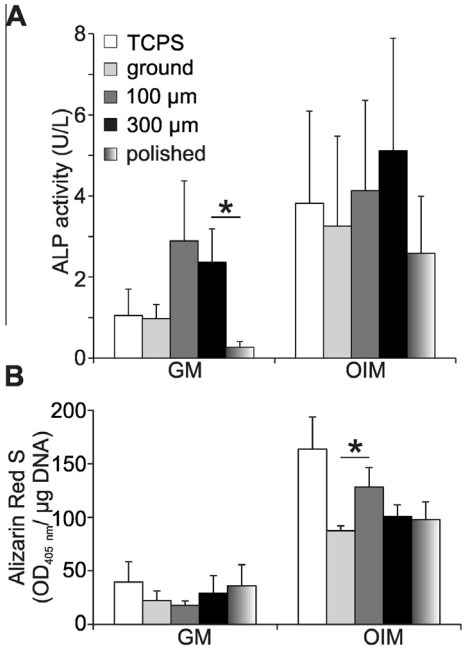

Fig. 6. Analysis of osteogenic differentiation after 21 days of stimulation. Three alumina samples per condition were cultivated with hMSCs for each donor experiment. (A) Alkaline phosphatase (ALP) activity. Supernatants of the cells were harvested to evaluate the ALP activity in duplicates. Bars represent averaged values ± standard error of the independent experiments with cells from four donors. *, $p < 0.05$, 300 µm vs. polished. (B) Calcium deposits stained by Alizarin Red S. Staining was solubilized and quantified from three independent donors. Absorbance at 405 nm was normalized to the DNA content in the lysate as measured by picoGreen. *, $p < 0.05$, 100 µm vs. ground ($R_a < 1.8$ µm).

However, secreted osteocalcin protein levels measured by an ELISA assay (Suppl. Fig. S5C) on the 300 µm spaced structures were similar to those of the TCPS positive control. Osteopontin protein levels measured by a Western Blot were only modestly affected (see Suppl. Fig. S5D). Inducing matrix mineralization by OIM revealed higher calcium contents compared to the ground and TCPS surfaces indicating that inkjet-printed micropatterns affect osteogenic differentiation. Furthermore, under growth medium conditions, the structure with 300 µm spaced pillars exhibited a significantly higher ALP enzyme activity compared to other surfaces. However, mineralization visualized by Alizarin Red S staining in the absence of osteogenic inducing agents (GM) was comparably low in all samples.

Please cite this article in press as: I. Lauria et al., Inkjet printed periodical micropatterns made of inert alumina ceramics induce contact guidance and stimulate osteogenic differentiation of mesenchymal stromal cells, Acta Biomater. (2016), http://dx.doi.org/10.1016/j.actbio.2016.08.004

To determine whether osteoblast differentiation could be triggered by the inkjet-printed topographies alone and without chemical induction [12,24,43], the cells were fed with OIM without dexamethasone (OIM-dex) for 21 days (Suppl. Fig. S6). With regards to ALP activity (Suppl. Fig. S6A), cells on microstructured surfaces exhibited higher values compared to TCPS or polished surfaces when cultured with GM or OIM-dex. Likewise, a similar trend was shown for the mineralization from these samples, which was highest on the 300 µm structure in comparison to polished and the other alumina samples (Suppl. Fig. S6B).

Furthermore, real-time PCR (qPCR) of the genes collagen I (COLI), RUNX2, ALP, and OPN normalized to beta-actin, comparing OIM and GM conditions at day 14 and 21, respectively, were conducted with three individual stem cell donors (Fig. 7A). To clarify whether the microtopography alone is able to stimulate osteoblast differentiation, RNA at day zero (starting day of induction) and at day seven was isolated for the subsequent qPCR analyses of two donors (see Fig. 7B). The COLI gene expression was slightly upregulated after 14 days of OIM treatment in all cells on the samples. However, after 21 days cells on ground alumina surfaces showed an increase of COLI compared to all other samples. Printed structures behaved similar to the positive control TCPS. Considering the early response of COLI gene expression, when compared to day zero, both donors behaved differently, one reacted to the ground and the other to the 100 µm structure. The gene expression level of RUNX2 was as high as on the TCPS control, whereas other alumina surfaces showed lower fold changes. Considering the early response of RUNX2 expression after seven days, donor 1 exhibited increased expression on all alumina samples with 100 µm distanced pillars showing the highest values, especially when cultured with GM. In contrast, donor 2 reacted to the ground surface with increased expression of RUNX2. Monitoring ALP expression after 21 days, the expression on all alumina samples was elevated compared to TCPS, in line with data after seven days and OIM. In addition, the early response of donor 1 indicated an influence of the 300 µm periodical micropattern, however donor 2 reacted more to the ground surface with increased expression of ALP. Regarding OPN (see Fig. 7A), on the positive control surface TCPS, gene expression was induced highest after 21 days of osteogenic induction. Ground surfaces showed the lowest fold changes of gene expression. After 14 days of osteogenic induction the 300 µm microstructures performed better, after 21 days both printed surfaces revealed increased fold ratios compared to ground specimens.

4. Discussion

Stem cells must react to their environment, which is important for the development of tissues and for the adaptation to certain circumstances like injuries, wounds or implant contact [44]. Cells respond by changing their initial adhesion, cell morphology and viability by stimulated cell division, migration or differentiation, thereby regulating the formation and regeneration of tissues. In addition to being controlled by chemical microenvironmental signals, in fact MSCs have been shown to be extremely sensitive to tissue-level elasticity [45] and topography [24], both of which are challenging to mimic with biomaterial surfaces [46]. A key tenet in bone tissue engineering is thus the development of scaffold materials that can stimulate stem cell differentiation in the absence of chemical treatment and without compromising material features [24].

In this study, we were aiming to tailor surfaces of alumina ceramics which as bioinert materials have excellent mechanical properties, however without modification they exhibit low

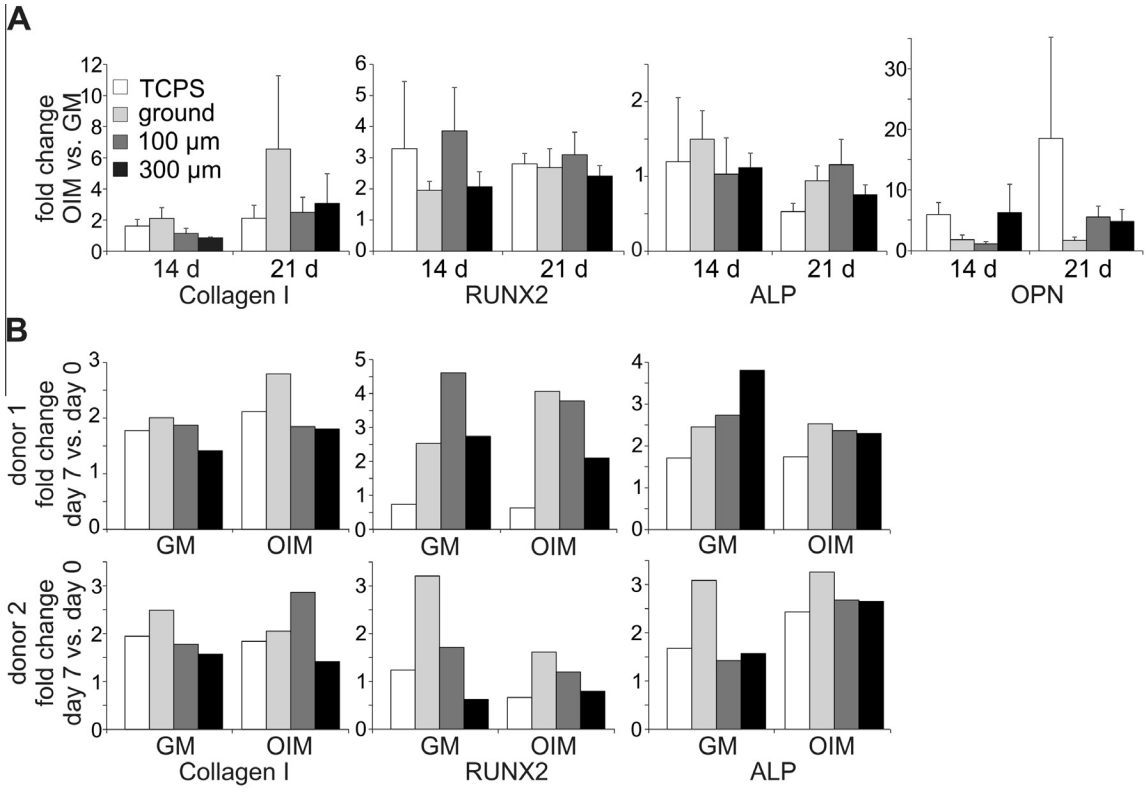

Fig. 7. Osteogenic marker gene expression measured by qPCR. Day zero refers to the start of osteogenic induction of hMSCs with OIM. Then, cells were cultured in parallel with GM or OIM for 14/21 (A) or 7 d (B). Bars represent means ± standard errors from three independent donor experiments performed with three alumina samples each measured in triplicates (A). In (B) averaged values of two individual donor experiments (donor 1 and 2) are depicted.

Please cite this article in press as: I. Lauria et al., Inkjet printed periodical micropatterns made of inert alumina ceramics induce contact guidance and stimulate osteogenic differentiation of mesenchymal stromal cells, Acta Biomater. (2016), http://dx.doi.org/10.1016/j.actbio.2016.08.004

Table 1
Summary of quantitatively measured cellular responses to printed structures.

	Viability 7 d	Alizarin	ALP protein	qPCR OPN
100 μm		+	(+)	(+)
300 μm	+		+	(+)

+, significantly increased; (+), not significant results; OPN: osteopontin.

osseointegration. Additive Manufacturing (AM) is a manufacturing technique used to construct 3D objects with high complexity through selective solidification of a layer-by-layer build-up of material based on a Computer-Aided Design (CAD) model [47]. For the production of dense, precise and detailed very small ceramic structures, DIP is the most promising technology and offers a variety of advantages in contrast to other AM techniques. For example, thermal inkjet print heads allow the use of solid contents of 27 vol% and more [36] in contrast to contents of 14.2 vol% with the piezoelectric ejection principle [31]. Furthermore, while conventional powder-bed-based 3D printing (3DP) and Selective Laser Sintering (SLS) solidify a powder bed according to different principles, DIP applies a drop-by-drop suspension directly through the print head nozzles. As a result, structures with high density are produced [36]. In contrast, 3DP and SLS generate structures yielding a porosity of approximately 40 vol% [48]. Stereo lithography (STL) produces ceramic bodies with theoretical densities of up to 98% with a lateral resolution of about 120 μm and 10 μm in the vertical direction [49], in comparison to Direct Inkjet Printing which yields comparable densities but higher lateral and vertical resolutions (45 μm × 45 μm × 5 μm). In summary, without changing the surface chemical composition, DIP generated micropillar arrays with periodicities of 100 and 300 μm (Fig. 1) which were tested for their influence on the stimulation of hMSC adhesion and osteogenic differentiation. Our quantitatively measured results are summarized in Table 1.

4.1. Micropatterns induce contact guidance of hMSCs

Using SEM, early after seeding hMSCs were observed connecting to and between the pillars (Fig. 2). The cell shape changed according to the periodical micropatterns. MSC were more branched compared to ground or polished alumina surfaces. The cells were in contact with many neighboring micropillars by their extensions. Consequently, patterned surfaces direct cell spatial dynamics in a process known as contact guidance, yielding cells oriented along the surface geometry [50,51]. Topographical cues are recognized and signals are transported potentially via the RhoA/ROCK pathway, a key modulator of both mesenchymal stem cell and osteoblast orientation on nanometric surface features [50]. Calzado-Martin et al. found that RhoA and its effector participate in the alignment of mesenchymal stem cells on submicrometric grooves but not of osteoblasts, implying the involvement of RhoA/ROCK signaling in contact guidance although to a varying extent depending on the specific cell type and the dimensions of the pattern.

Although we did not study RhoA/ROCK signaling, we found MSCs being oriented or aligned along and also connecting between two pillars. However, this occurred only partially with MG-63 (Suppl. Fig. S2B/D), and L-929 (data not shown) did not display such a cell morphology. Both cell types exhibit smaller sizes of their cell bodies compared to hMSCs. It can be hypothesized that the printed microstructures may not influence the response of MG-63 or L-929, which is supported by our viability measurements. The metabolic activity of both cell lines was not significantly affected by the microstructuring (Suppl. Fig. S2A). However, Fig. 5 depicts a trend to higher activity when hMSCs were seeded onto structured surfaces. In particular, at day seven and when comparing polished (R_a < 0.2 μm) and ground (R_a < 1.8 - μm) or printed surfaces, the ground and 300 μm spaced printed arrays produced significantly higher cell viabilities (see also Table 1 for comparison). In other studies, rough material surfaces yielded varying results in cell viability tests. A recent study revealed an increase of mesenchymal stem cell numbers on polycaprolactone with $R_a \sim 1.5$ μm [43], a roughness value similar to our ground alumina surfaces (R_a < 1.8 μm), however others verified decreasing metabolic activities of osteoblast cells at least to some extent for R_a < 0.83 μm [52], 0.9 μm [53], or 2.19 μm [54]. In conclusion, on polished alumina surfaces (R_a < 0.2 μm) cell viability is low. Instead, ground alumina (R_a < 1.8 μm) promotes the cell viability. The 300 μm printed microstructures additionally stimulate the proliferation of hMSC which is in line also with the work of Berry et al. [55]. The 100 μm structure yielded less viability compared to the 300 μm distanced pillars possibly due to the exposure of cells to less rough surface area. Again, the measured cell response strongly depends on the material, topography and the cell type used in the study [11,50,55,56]. Taken together, the human mesenchymal stromal cells respond to the inkjet-printed microstructures by contact guidance and exhibit significantly increased viability after seven days on the 300 μm spaced pillar surfaces.

4.2. Pillars induce focal adhesion dependent cell attachment

Approximately at day seven, cells were situated on the micropillars (Fig. 2). Besides the RhoA/ROCK pathway focal adhesions (FAs) have also been implicated in the reactions of cells to micro- or nanotopography [57–61]. When we immunofluorescently labeled the FA proteins integrin-β5, vinculin, and FAK at day five (Fig. 4), the presence of FAs was confirmed [57,58]. All three stainings illustrated focal adhesions localized on the micropillar demonstrating cells being directly attached to the microstructures, thereby proving pillar mediated cell adhesion. Whether this changed adhesion and cell shape correlates with an elevated integrin β1 expression level, as shown on nanoporous alumina [22], has to be elucidated. The speed of cell migration [55], quantified as the focal adhesion area and life span [62–64], could be changed on substrate microtopographies with varying dimensions or compared to flat surfaces. Frey et al. observed a zigzag migration of fibroblasts on pillared substrates and suggested that FAK-dependent contractile forces drag cells from one pillar to another [64]. Ghibaudo et al. analyzed the migration behavior of fibroblasts on micropillar substrates aiming to mimic a 3D environment as present in tissues [63]. They observed cells being more elongated and branched compared with cells on flat specimens. In addition, they found different migration mechanisms including a persistent type of 3D migration which depends on the organization and dimensions of topographical features. It has to be further investigated whether this migration phenotype is also present on the printed pillar arrays. Moreover, it remains elusive whether this also affects cell viability as displayed in Fig. 5. Along with spatial reorganization of the actin cytoskeleton, a preferential formation of FA on the micropillar with an increased lifetime was demonstrated. Analogous to the effects described here, it appears that micropillars made of alumina promote the guidance of hMSC actin fibers (Fig. 4). Moreover, FAs were preferentially localized on the pillars. Since FA are known to regulate traction forces [65], it can be speculated that FA drive the directionality of cell movement onto our printed alumina micropillars. Thus, DIP generated microstructures promote pillar-mediated adhesion and possibly direct the migration of hMSCs thereby creating a situation closer to *in vivo* 3D cell behavior in the body. After 21 days, cells are able to construct a 3D environment built up of anorganic micropillars and organic cell mass with highest cell viabilities, as suggested by the findings presented in Fig. 5B.

Please cite this article in press as: I. Lauria et al., Inkjet printed periodical micropatterns made of inert alumina ceramics induce contact guidance and stimulate osteogenic differentiation of mesenchymal stromal cells, Acta Biomater. (2016), http://dx.doi.org/10.1016/j.actbio.2016.08.004

4.3. Osteogenic differentiation of hMSCs

Despite revealing only modest differences in osteocalcin secretion measured by ELISA (see Suppl. Fig. S5C), osteopontin protein level visualized by a Western Blot (Suppl. Fig. S5D), and in ALP activities of hMSCs cultured with OIM, cells on the 300 μm structure exhibited significantly elevated ALP activities when cultured with GM (Fig. 6A, Table 1). This finding is supported by results presented in Suppl. Fig. S6A which shows that under GM conditions printed surfaces raised the ALP activity of hMSCs. When we tested Faia-Torres' hypothesis that rough surfaces are able to induce osteogenic differentiation per se, i.e. in the absence of dexamethasone (OIM-dex) [43] we observed increasing levels of ALP not only on our ground alumina specimens with R_a < 1.8 μm but also on our printed surfaces compared to the polished control (Suppl. Fig. S6A). As expected, the activities of cells on TCPS were not affected. Printed surfaces consistently yielded the strongest ALP activities. Similarly, others also observed increasing ALP protein or gene levels on micro- or nanostructured alumina [22,25,66,67]. Comparing ALP gene expression at day seven (Fig. 7B), microstructured surfaces stimulated gene expression, however a detailed observation reveals a donor specific reaction of ALP expression to the surfaces used here. In summary, considering the marker ALP, our results indicate that submicrometer structures on the ground surface combined with micrometer-sized structures as presented by our micropillar arrays can induce ALP gene expression yielding elevated protein levels in the cell supernatants, most importantly without chemical induction by dexamethasone.

In addition to the ALP gene expression, collagen I and RUNX2 also showed donor specific reactions to the various alumina surfaces. The RUNX2 expression of donor 1 was strongly elevated compared to the TCPS control (Fig. 7B). In growth medium, the 100 μm micropillars revealed the highest fold changes, whereas donor 2 exhibited the highest RUNX2 on ground surfaces. Our findings are supported by other studies on microstructured alumina which observed higher levels of RUNX2 [25]. The signaling cascades involved in our study might be numerous. Dexamethasone treatment induces ALP expression and COLI expression in all samples, however RUNX2 expression seems to be induced even more suggesting an additive effect of the topographical cues of our alumina samples as hypothesized by Watari et al. [68]. When cultured without chemical induction, RUNX2 expression was also enhanced, especially on the 100 μm and ground surface. RUNX2 is a transcription factor regulating the gene expression of, for example, other osteoblast matrix proteins like osteocalcin, and it requires post-translational modification of itself. Obviously, these pathways leading to the activation of RUNX2 also have to be induced. As additional late osteogenic marker, we studied the expression of OPN (Fig. 7A). Though osteocalcin and osteopontin proteins were only slightly affected (Suppl. Fig. S5C/D), and other gene expression analyses of other genes showed only donor individual responses, OPN mean fold ratios were increased on the printed surfaces (Table 1). In line with another report analyzing the response of human mesenchymal stem cells to topographical cues [62], we did not observe significant differences of gene expression. It can be hypothesized that donor-specific variations, as demonstrated in these studies, necessitate higher numbers of biological replicas yielding results with statistical significance.

Besides gene expression and protein levels of certain markers, osteogenic differentiation is confirmed by matrix mineralization which was visualized by SEM/EDX (Suppl. Fig. S5B) and stained by ARS and quantified (Fig. 6B/Suppl. Fig. S5A). According to Kim et al. [25] and Wilkinson et al. [69], cellular response is restricted to a specific dimension. In fact, when hMSCs were cultured on the microstructured alumina surfaces, the 100 μm micropattern exhibited significantly higher calcium contents compared to the ground surface. OIM without dexamethasone yielded a trend to higher mineralization when compared to the less structured polished surface, supporting Faia-Torres' hypothesis [43]. Taken together, our results indicate that micropillar arrays made of alumina are able to stimulate osteogenic differentiation.

5. Conclusion

Employing thermal DIP manufacturing technique, we generated micropillar arrays with two dimensions made out of bioinert alumina ceramics. We found that human MSC respond to the microstructured surfaces by contact guidance and increased cell viability after seven days. In addition, we could see focal adhesions on the micropillars the existence of which proves microstructure-mediated and FA-dependent cell adhesion and indicates directed cell movement onto the micropillars. With regards to marker gene expression, though varying donor specific results were observed, in particular ALP and RUNX2 were induced without chemical induction by dexamethasone. The late osteogenic marker OPN could be stimulated on the inkjet printed alumina micropillared substrates, and finally, mineralization was enhanced on one of the periodical micropatterns. It can be concluded that bioinert alumina can be bioactivated by DIP without any chemical modification only by topographical cues. Furthermore, cells utilize the microstructures for the generation of a 3D environment composed of inorganic micropillars and organic cell mass.

Disclosure

The authors do not have any conflicts of interest to disclose.

Acknowledgments

The authors acknowledge the financial support of this study by the AIF (German Federation of Industrial Research Associations, Grant number: 493 ZN). We are grateful to Stephan Rütten, Institute of Pathology, RWTH Aachen University Hospital for his help with the SEM analysis. We thank Roswitha Davtalab, Michael Weber, Franz Jungwirth, and Marie Isabelle Zulka, all Department of Dental Materials and Biomaterials Research, RWTH Aachen University Hospital, for their technical support.

Appendix A. Supplementary data

Supplementary data associated with this article can be found, in the online version, at http://dx.doi.org/10.1016/j.actbio.2016.08.004.

References

[1] P. Griss, E. Werner, G. Heimke, Alumina ceramic, bioglass and silicon nitride. A comparative biocompatibility study, Mech. Prop. Biomater. (1978).
[2] G. Maccauro, P. Iommetti, L. Raffaelli, P. Manicone, Alumina and zirconia ceramic for orthopaedic and dental devices, Biomater. Appl. Nanomed. (2011) 299–308.
[3] O. Roualdes, M.-E. Duclos, D. Gutknecht, L. Frappart, J. Chevalier, D.J. Hartmann, In vitro and in vivo evaluation of an alumina–zirconia composite for arthroplasty applications, Biomaterials 31 (2010) 2043–2054.
[4] R. Depprich, H. Zipprich, M. Ommerborn, C. Naujoks, H.-P. Wiesmann, S. Kiattavorncharoen, H.-C. Lauer, U. Meyer, N.R. Kübler, J. Handschel, Osseointegration of zirconia implants compared with titanium: an in vivo study, Head Face Med. 4 (2008) 30.
[5] B.J. McEntire, B.S. Bal, M.N. Rahaman, J. Chevalier, G. Pezzotti, Ceramics and ceramic coatings in orthopaedics, J. Eur. Ceram. Soc. 35 (2015) 4327–4369.
[6] H. Fischer, C. Niedhart, N. Kaltenborn, A. Prange, R. Marx, F.U. Niethard, R. Telle, Bioactivation of inert alumina ceramics by hydroxylation, Biomaterials 26 (2005) 6151–6157.
[7] F. Böke, K. Schickle, H. Fischer, Biological activation of inert ceramics: recent advances using tailored self-assembled monolayers on implant ceramic surfaces, Materials (Basel). 7 (2014) 4473–4492.

[8] Y. Song, Y. Ju, Y. Morita, B. Xu, G. Song, Surface functionalization of nanoporous alumina with bone morphogenetic protein 2 for inducing osteogenic differentiation of mesenchymal stem cells, Mater. Sci. Eng. C. Mater. Biol. Appl. 37 (2014) 120–126.
[9] A. Aminian, K. Pardun, E. Volkmann, G. Li Destri, G. Marletta, L. Treccani, K. Rezwan, Enzyme-assisted calcium phosphate biomineralization on an inert alumina surface, Acta Biomater. 13 (2014) 335–343.
[10] K. Schickle, A. Korsten, M. Weber, C. Bergmann, S. Neuss, H. Fischer, Towards osseointegration of bioinert ceramics: can biological agents be immobilized on alumina substrates using self-assembled monolayer technique?, J Eur. Ceram. Soc. 33 (2013) 2705–2713.
[11] X. Le, G.E.J. Poinern, N. Ali, C.M. Berry, D. Fawcett, Engineering a biocompatible scaffold with either micrometre or nanometre scale surface topography for promoting protein adsorption and cellular response, Int. J. Biomater. 2013 (2013) 782549.
[12] L.E. McNamara, R. Burchmore, M.O. Riehle, P. Herzyk, M.J.P. Biggs, C.D.W. Wilkinson, A.S.G. Curtis, M.J. Dalby, The role of microtopography in cellular mechanotransduction, Biomaterials 33 (2012) 2835–2847.
[13] M. Karlsson, E. Pålsgård, P. Wilshaw, L. Di Silvio, Initial in vitro interaction of osteoblasts with nano-porous alumina, Biomaterials 24 (2003) 3039–3046.
[14] M. Wieland, M. Textor, B. Chehroudi, D.M.D.M. Brunette, Synergistic interaction of topographic features in the production of bone-like nodules on Ti surfaces by rat osteoblasts, Biomaterials 26 (2005) 1119–1130.
[15] K. Anselme, A. Ponche, M. Bigerelle, Relative influence of surface topography and surface chemistry on cell response to bone implant materials. Part 2: biological aspects, Proc. Inst. Mech. Eng. Part H J. Eng. Med. 224 (2010) 1487–1507.
[16] L. Le Guéhennec, A. Soueidan, P. Layrolle, Y. Amouriq, Surface treatments of titanium dental implants for rapid osseointegration, Dent. Mater. 23 (2007) 844–854.
[17] I. Wittenbrink, A. Hausmann, K. Schickle, I. Lauria, R. Davtalab, M. Foss, A. Keller, H. Fischer, Low-aspect ratio nanopatterns on bioinert alumina influence the response and morphology of osteoblast-like cells, Biomaterials 62 (2015) 58–65.
[18] S. Neuss, C. Panfil, D.F. Duarte Campos, M. Weber, C. Otten, U. Reisgen, H. Fischer, Adhesion of human mesenchymal stem cells can be controlled by electron beam-microstructured titanium alloy surfaces during osteogenic differentiation, Biomed. Tech. (Berl) 60 (2015) 215–223.
[19] J. Zhang, X. Luo, D. Barbieri, A.M.C. Barradas, J.D. de Bruijn, C.A. van Blitterswijk, H. Yuan, The size of surface microstructures as an osteogenic factor in calcium phosphate ceramics, Acta Biomater. 10 (2014) 3254–3263.
[20] M. Echeverry-Rendón, O. Galvis, D. Quintero Giraldo, J. Pavón, J.L. López-Lacomba, E. Jiménez-Piqué, M. Anglada, S.M. Robledo, J.G. Castaño, F. Echeverría, Osseointegration improvement by plasma electrolytic oxidation of modified titanium alloys surfaces, J. Mater. Sci. Mater. Med. 26 (2015) 72.
[21] B.J. Pedimonte, T. Moest, T. Luxbacher, C. von Wilmowsky, T. Fey, K.A. Schlegel, P. Greil, Morphological zeta-potential variation of nanoporous anodic alumina layers and cell adherence, Acta Biomater. 10 (2014) 968–974.
[22] Y. Song, Y. Ju, G. Song, Y. Morita, In vitro proliferation and osteogenic differentiation of mesenchymal stem cells on nanoporous alumina, Int. J. Nanomed. 8 (2013) 2745–2756.
[23] D. Nadeem, T. Sjostrom, A. Wilkinson, C.-A. Smith, R.O.C. Oreffo, M.J. Dalby, B. Su, Embossing of micropatterned ceramics and their cellular response, J. Biomed. Mater. Res. A. 101 (2013) 3247–3255.
[24] M.J. Dalby, N. Gadegaard, R. Tare, A. Andar, M.O. Riehle, P. Herzyk, C.D.W. Wilkinson, R.O.C. Oreffo, The control of human mesenchymal cell differentiation using nanoscale symmetry and disorder, Nat. Mater. 6 (2007) 997–1003.
[25] S.-Y. Kim, J.-H. Kang, W.-S. Seo, S.-W. Lee, N.-S. Oh, H.-K. Cho, M.-H. Lee, Effect of topographical control by a micro-molding process on the activity of human Mesenchymal Stem Cells on alumina ceramics, Biomater. Res. 19 (2015) 23.
[26] R.J. Kohal, M. Bächle, A. Renz, F. Butz, Evaluation of alumina toughened zirconia implants with a sintered, moderately rough surface. An experiment in the rat, Dent. Mater. (2015).
[27] J.A. Lewis, J.E. Smay, J. Stuecker, J. Cesarano, Direct ink writing of three-dimensional ceramic structures, J. Am. Ceram. Soc. 89 (2006) 3599–3609.
[28] S.F.S. Shirazi, S. Gharehkhani, M. Mehrali, H. Yarmand, H.S.C. Metselaar, N. Adib Kadri, N.A.A. Osman, A review on powder-based additive manufacturing for tissue engineering: selective laser sintering and inkjet 3D printing, Sci. Technol. Adv. Mater. 16 (2015) 033502.
[29] B. Derby, Inkjet printing ceramics: from drops to solid, J. Eur. Ceram. Soc. 31 (2011) 2543–2550.
[30] E. Özkol, J. Ebert, R. Telle, An experimental analysis of the influence of the ink properties on the drop formation for direct thermal inkjet printing of high solid content aqueous 3Y-TZP suspensions – 1-s2.0-S0955221910000087-main.pdf, J. Eur. Ceram. Soc. 30 (2010) 1669–1678.
[31] X. Zhao, J.R.G. Evans, M.J. Edirisinghe, J.H. Song, Ink-jet printing of ceramic pillar arrays, J. Mater. Sci. 37 (2002) 1987–1992.
[32] A.V. Kumar, A. Dutta, J.E. Fay, Electrophotographic printing of part and binder powders, Rapid Prototype J. 10 (2004) 7–13.
[33] X. Cui, T. Boland, D.D. D'Lima, M.K. Lotz, Thermal inkjet printing in tissue engineering and regenerative medicine, Recent Pat. Drug Delivery Formul. 6 (2012) 149–155.
[34] P. Mareike Wätjen, M. Gingter, M. Kramer, R. Telle, Novel prospects and possibilities in additive manufacturing of ceramics by means of direct inkjet printing, Adv. Mech. Eng. 2014 (2014) 1–12 (Hindawi Publ. Corp.).
[35] P. Gingter, A. Wätjen, M. Kramer, R. Telle, Functionally graded ceramic structures by direct thermal inkjet printing, J. Ceram. Sci. Technol. 6 (2015) 119–124.
[36] J. Ebert, E. Ozkol, A. Zeichner, K. Uibel, O. Weiss, U. Koops, R. Telle, H. Fischer, Direct inkjet printing of dental prostheses made of zirconia, J. Dent. Res. 88 (2009) 673–676.
[37] C.L. Ventola, Medical Applications for 3D Printing: Current and Projected Uses., P T. 39 (2014) 704–11.
[38] R.K. Schneider, J. Anraths, R. Kramann, J. Bornemann, M. Bovi, R. Knüchel, S. Neuss, The role of biomaterials in the direction of mesenchymal stem cell properties and extracellular matrix remodelling in dermal tissue engineering, Biomaterials 31 (2010) 7948–7959.
[39] R.K. Schneider, A. Puellen, R. Kramann, K. Raupach, J. Bornemann, R. Knuechel, A. Pérez-Bouza, S. Neuss, The osteogenic differentiation of adult bone marrow and perinatal umbilical mesenchymal stem cells and matrix remodelling in three-dimensional collagen scaffolds, Biomaterials 31 (2010) 467–480.
[40] G.R. Nakayama, M.C. Caton, M.P. Nova, Z. Parandoosh, Assessment of the Alamar Blue assay for cellular growth and viability in vitro, J. Immunol. Methods 204 (1997) 205–208.
[41] M.W. Pfaffl, A new mathematical model for relative quantification in real-time RT-PCR, Nucleic Acids Res. 29 (2001) e45.
[42] D.F. Duarte Campos, A. Blaeser, A. Korsten, S. Neuss, J. Jäkel, M. Vogt, H. Fischer, The stiffness and structure of three-dimensional printed hydrogels direct the differentiation of mesenchymal stromal cells toward adipogenic and osteogenic lineages, Tissue Eng. Part A (2015).
[43] A.B. Faia-Torres, M. Charnley, T. Goren, S. Guimond-Lischer, M. Rottmar, K. Maniura-Weber, N.D. Spencer, R.L. Reis, M. Textor, N.M. Neves, Acta biomaterialia osteogenic differentiation of human mesenchymal stem cells in the absence of osteogenic supplements: a surface-roughness gradient study, Acta Biomater. 28 (2015) 1–12.
[44] A. Uccelli, L. Moretta, V. Pistoia, Mesenchymal stem cells in health and disease, Nat. Rev. Immunol. 8 (2008) 726–736.
[45] A.J. Engler, S. Sen, H.L. Sweeney, D.E. Discher, Matrix elasticity directs stem cell lineage specification, Cell 126 (2006) 677–689.
[46] M.F. Griffin, P.E. Butler, A.M. Seifalian, D.M. Kalaskar, Control of stem cell fate by engineering their micro and nanoenvironment, World J. Stem Cells. 7 (2015) 37–50.
[47] F.E.H. Tay, A. Roy, CyberCAD: a collaborative approach in 3D-CAD technology in a multimedia-supported environment, Comput. Ind. 52 (2003) 127–145.
[48] N. Travitzky, A. Bonet, B. Dermeik, T. Fey, I. Filbert-Demut, L. Schlier, T. Schlordt, P. Greil, Additive manufacturing of ceramic-based materials, Adv. Eng. Mater. 16 (2014) 729–754.
[49] C. Chaput, T. Chartier, Fabrication of ceramics by stereolithography, RTe J. Forum Für Rapid Technol. 4 (2007).
[50] A. Calzado-Martín, A. Méndez-Vilas, M. Multigner, L. Saldaña, J.L. González-Carrasco, M.L. González-Martín, N. Vilaboa, On the role of RhoA/ROCK signaling in contact guidance of bone-forming cells on anisotropic Ti6Al4V surfaces, Acta Biomater. 7 (2011) 1890–1901.
[51] R. McBeath, D.M. Pirone, C.M. Nelson, K. Bhadriraju, C.S. Chen, Cell shape, cytoskeletal tension, and RhoA regulate stem cell lineage commitment, Dev. Cell 6 (2004) 483–495.
[52] G. Zhao, A.L. Raines, M. Wieland, Z. Schwartz, B.D. Boyan, Requirement for both micron- and submicron scale structure for synergistic responses of osteoblasts to substrate surface energy and topography, Biomaterials 28 (2007) 2821–2829.
[53] L. Saldaña, L. Crespo, F. Bensiamar, M. Arruebo, N. Vilaboa, Mechanical forces regulate stem cell response to surface topography, J. Biomed. Mater. Res. A. 102 (2014) 128–140.
[54] K. Anselme, P. Linez, M. Bigerelle, D. Le Maguer, A. Le Maguer, P. Hardouin, H.F. Hildebrand, A. Iost, J.M. Leroy, The relative influence of the topography and chemistry of TiAl6V4 surfaces on osteoblastic cell behaviour, Biomaterials 21 (2000) 1567–1577.
[55] C.C. Berry, G. Campbell, A. Spadiccino, M. Robertson, A.S.G. Curtis, The influence of microscale topography on fibroblast attachment and motility, Biomaterials 25 (2004) 5781–5788.
[56] M.P. Lutolf, P.M. Gilbert, H.M. Blau, Designing materials to direct stem-cell fate, Nature 462 (2009) 433–441.
[57] B. Geiger, J.P. Spatz, A.D. Bershadsky, Environmental sensing through focal adhesions, Nat. Rev. Mol. Cell Biol. 10 (2009) 21–33.
[58] J.D. Humphries, P. Wang, C. Streuli, B. Geiger, M.J. Humphries, C. Ballestrem, Vinculin controls focal adhesion formation by direct interactions with talin and actin, J. Cell Biol. 179 (2007) 1043–1057.
[59] C.H. Seo, K. Furukawa, K. Montagne, H. Jeong, T. Ushida, The effect of substrate microtopography on focal adhesion maturation and actin organization via the RhoA/ROCK pathway, Biomaterials 32 (2011) 9568–9575.
[60] A. Diener, B. Nebe, F. Lüthen, P. Becker, U. Beck, H.G. Neumann, J. Rychly, Control of focal adhesion dynamics by material surface characteristics, Biomaterials 26 (2005) 383–392.
[61] B.K.K. Teo, S.T. Wong, C.K. Lim, T.Y.S. Kung, C.H. Yap, Y. Ramagopal, L.H. Romer, E.K.F. Yim, Nanotopography modulates mechanotransduction of stem cells and induces differentiation through focal adhesion kinase, ACS Nano 7 (2013) 4785–4798.
[62] G. Abagnale, M. Steger, V.H. Nguyen, N. Hersch, A. Sechi, S. Joussen, B. Denecke, R. Merkel, B. Hoffmann, A. Dreser, U. Schnakenberg, A. Gillner, W. Wagner, Surface topography enhances differentiation of mesenchymal stem cells towards osteogenic and adipogenic lineages, Biomaterials 61 (2015) 316–326.

Please cite this article in press as: I. Lauria et al., Inkjet printed periodical micropatterns made of inert alumina ceramics induce contact guidance and stimulate osteogenic differentiation of mesenchymal stromal cells, Acta Biomater. (2016), http://dx.doi.org/10.1016/j.actbio.2016.08.004

[63] M. Ghibaudo, L. Trichet, J. Le Digabel, A. Richert, P. Hersen, B. Ladoux, Substrate topography induces a crossover from 2D to 3D behavior in fibroblast migration, Biophys. J. 97 (2009) 357–368.
[64] M.T. Frey, I.Y. Tsai, T.P. Russell, S.K. Hanks, Y.-L. Wang, Cellular responses to substrate topography: role of myosin II and focal adhesion kinase, Biophys. J. 90 (2006) 3774–3782.
[65] D. Riveline, E. Zamir, N.Q. Balaban, U.S. Schwarz, T. Ishizaki, S. Narumiya, Z. Kam, B. Geiger, A.D. Bershadsky, Focal contacts as mechanosensors: externally applied local mechanical force induces growth of focal contacts by an mdia1-dependent and rock-independent mechanism, J. Cell Biol. 153 (2001) 1175–1186.
[66] W. Metzger, B. Schwab, M.M. Miro, S. Grad, A. Simpson, M. Veith, G. Wennemuth, V. Zaporojtchenko, S. Verrier, J.S. Hayes, M. Bubel, T. Pohlemann, M. Oberringer, C. Aktas, Induction of osteogenic differentiation by nanostructured alumina surfaces, J. Biomed. Nanotechnol. 10 (2014) 831–845.
[67] K.C. Popat, K.-I. Chatvanichkul, G.L. Barnes, T.J. Latempa, C.A. Grimes, T.A. Desai, Osteogenic differentiation of marrow stromal cells cultured on nanoporous alumina surfaces, J. Biomed. Mater. Res. A. 80 (2007) 955–964.
[68] S. Watari, K. Hayashi, J.A. Wood, P. Russell, P.F. Nealey, C.J. Murphy, D.C. Genetos, Modulation of osteogenic differentiation in hMSCs cells by submicron topographically-patterned ridges and grooves, Biomaterials 33 (2012) 128–136.
[69] A. Wilkinson, R.N. Hewitt, L.E. McNamara, D. McCloy, R.M. Dominic Meek, M.J. Dalby, Biomimetic microtopography to enhance osteogenesis in vitro, Acta Biomater. 7 (2011) 2919–2925.

Please cite this article in press as: I. Lauria et al., Inkjet printed periodical micropatterns made of inert alumina ceramics induce contact guidance and stimulate osteogenic differentiation of mesenchymal stromal cells, Acta Biomater. (2016), http://dx.doi.org/10.1016/j.actbio.2016.08.004